Journal of the Ceramic Society of Japan 121 [8] 710-713 2013 Paper

Anisotropic growth of zinc oxide pillars on silver nanoparticles by oblique angle deposition

Shunsuke MURAI,[*,†] Tomohiko MATOBA,[*,] Christopher T. NELSON,[**] Takuya KOMINE,[*] Koji FUJITA,[*] Xiaoqing PAN[**] and Katsuhisa TANAKA[*]**

[*]**Department of Material Chemistry, Graduate School of Engineering, Kyoto University, Katsura, Nishikyo-ku, Kyoto 615–8510, Japan**

[**]**Department of Materials Science and Engineering, University of Michigan, Ann Arbor, MI 48109, USA**

We have prepared composites with anisotropic microstructure consisting of silver nanoparticles and zinc oxide pillars using an oblique angle deposition technique, and examined the optical response originating from their anisotropic morphology. The sample was obtained in three steps. First, the assembly of silver nanoparticles was prepared on a silica glass substrate by electron-beam deposition of the silver thin film and subsequent heat treatment. Next, zinc oxide was obliquely grown by using a pulsed laser deposition. Finally the zinc oxide was crystallized by the post annealing to make an array of inclined pillars grown on the top of the silver nanoparticles. The structure and morphology of the composites were elucidated by a combination of X-ray diffraction analysis and transmission electron microscopy. Optical rotation spectroscopy clarifies that the composite shows optical birefringence due to its inclined pillar morphology. The optical rotation spectrum exhibits two peaks, one being associated to the localized surface plasmon resonance of the silver nanoparticles and the other the excitons in the zinc oxide pillars. The present fabrication method is simple and can be applied to obtain anisotropic composites with relatively large dimensions.

Key-words : Oblique angle deposition, Plasmonics

[Received April 17, 2013; Accepted May 29, 2013]

1. Introduction

An electromagnetic wave incident on a metallic nanoparticle excites collective oscillation of the conduction electrons in the particle, known as localized surface plasmon resonances (LSPRs).[1)] The condition for the resonance varies with the shape of the particle, and anisotropic nanoparticles show responses which depend on their orientation relative to the incident light. A typical example is a metallic nanorod, which has two distinct conditions of resonance corresponding to two characteristic lengths due to its anisotropic shape. Assembling such anisotropic particles so that the axes of anisotropy are oriented parallel to each other gives rise to an assembly whose macroscopic optical response depends on the propagation direction and the polarization state of the incident light. Such materials can potentially be used not only as polarizers[2)] but also as metamaterials,[3),4)] which show the magnetic response or a negative index of refraction in a spectral region of interest. Assemblies of anisotropic particles can be made by electron-beam lithography with dimensions typically on the order of 100 μm × 100 μm.[4),5)] For larger scale fabrication, a colloidal template technique is broadly implemented, in which a self-assembled monolayer of colloidal spheres is used as a template for further processing of the microstructure.[6),7)] A variety of anisotropic morphologies are achievable by obliquely depositing metallic species onto the template.

The nanostructured systems mentioned above generally consist of anisotropic metal components embedded in an isotropic medium. An alternative way to achieve anisotropic response macroscopically is to embed isotropic nanoparticles into an anisotropic medium. Following this strategy, we have recently fabricated a composite of silver (Ag) nanoparticles and an iron oxide thin film.[8)] Ag nanoparticles made by heating Ag film on silica (SiO_2) glass substrate have no shape anisotropy or preferred orientations. The oblique deposition of iron oxide produces ellipsoidal shells surrounding the Ag nanoparticles, thus giving an anisotropic environment to the particles. This in-plane anisotropy of the composite is reflected in its optical response; the composite shows the LSPRs that vary with the polarization direction of incident light, and it manifests an optical birefringence around the LSPRs wavelength.[8)] This technique is versatile and allows fabrication of composites with any combination of metals and oxides with dimensions up to wafer-size.

In the present study, we have fabricated a composite of Ag nanoparticles and zinc oxide (ZnO) pillars by using the oblique angle deposition and post annealing. ZnO is selected because of its tendency of *c*-axis oriented growth, which presumably contributes to enhance optical anisotropy. In addition, the combination of ZnO with Ag leads to enhanced photoluminescence[9)] and photocatalytic effect.[10)] The anisotropic ZnO pillars/isotropic Ag particles geometry has been confirmed by transmission electron microscopy (TEM). We have further elucidated the influence of anisotropic morphology on the macroscopic optical response through the optical extinction and optical rotation measurements. The composites exhibit the enhanced optical birefringence around the spectral regions of the excitons of ZnO pillars and the LSPRs of Ag nanoparticles.

2. Experimental

2.1 Sample preparation

Ag thin films (thickness ~50 nm) were grown on SiO_2 glass substrates (7.5 mm × 7.5 mm × 0.5 mm) by using electron-beam

† Corresponding author: S. Murai; E-mail: murai@dipole7.kuic.kyoto-u.ac.jp

DOI http://dx.doi.org/10.2109/jcersj2.121.710

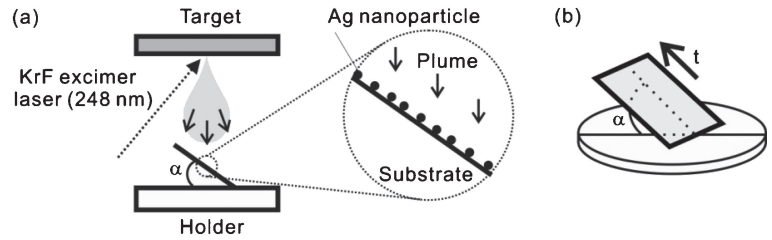

Fig. 1. (a) Schematic representation of the geometry for pulsed laser deposition using a tilted substrate with respect to the holder that is placed to face the target. A magnified illustration of the substrate is shown in the right circle. (b) A spatial relation of the holder and the substrate. The definitions of α and t are indicated.

deposition. The film thus obtained was heat-treated at 300°C in air for 5 min to convert the Ag film into an assembly of Ag nanoparticles. By using a pulsed laser deposition (PLD) method, ZnO pillars were grown onto the Ag nanoparticles placed on the SiO_2 glass substrate. A sintered body of ZnO was used as a target material. A sketch of the PLD geometry is shown in **Fig. 1**(a). The substrate was maintained at room temperature, the oxygen pressure was 1.0×10^{-4} Pa, and the distance between the target and the substrate was 2.5 cm. A KrF excimer laser (248 nm, 2 Hz) was focused on the target at a fluence of 1.65 J/cm^2. The deposition time was fixed to 30 min. The surface of the substrate was tilted with respect to the surface of the target by an angle of α, and the direction of the tilt on the substrate was defined as t, which makes an angle of α with respect to the holder [see Fig. 1(b)]. The deposition was carried out at two angles of $\alpha = 0$ and 60°. The as-deposited composites were annealed at 500°C in air for 10 min.

2.2 Structural characterization

X-ray diffraction (XRD) measurements were carried out with Cu Kα radiation (Rint2500, Rigaku) to identify crystalline phases precipitated in the resultant composites. A grazing incidence configuration was used to obtain a high surface sensitivity. An aberration-corrected STEM (JEOL 2100F with probe correction) equipped with a high angle annular dark field (HAADF) detector was used to characterize the cross-section of the film in the direction parallel to t, i.e., the direction of the tilt, and a high-resolution TEM (JEOL 3011) equipped with selected area electron diffraction (SAED) was utilized to obtain information on the cross-section perpendicular to t.

2.3 Optical characterization

The optical extinction was measured by using a spectral photometer (JASCO V-570) with the light source being unpolarized. Optical birefringence was evaluated by using a rotation of the polarization plane of linearly polarized light transmitted through the composite. For the measurement, a magneto-optical effect evaluation system (JASCO K-250) was utilized at zero magnetic field. Linearly polarized light was normally incident on the composite surface with a square spot size of ~2 mm × 2 mm, and the rotation angle of the polarization plane of the transmitted light, ξ, was detected by using a polarization modulation technique.[8] The angle between t on the substrate and the oscillation direction of the incident electric field was defined as azimuth Φ (see **Fig. 2**).

3. Results and discussion

3.1 Structure development by the oblique angle deposition and post annealing

Figure 3 shows the out-of-plane XRD patterns for the annealed composites. All the samples show diffraction peaks

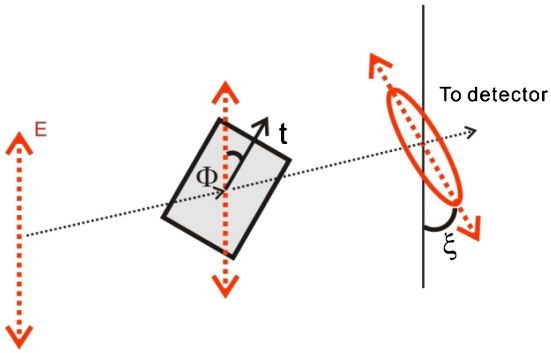

Fig. 2. Schematic representation of the experimental setup for the measurement of optical rotation. A linearly polarized light with electric field oscillating vertically was normally incident on the composite sample, and rotation angle of the polarization plane ξ of transmitted light was detected. The sample was rotated around an axis normal to the surface, and the angle between the direction of t on the substrate and that of the oscillating electric field of the incoming light was defined as Φ.

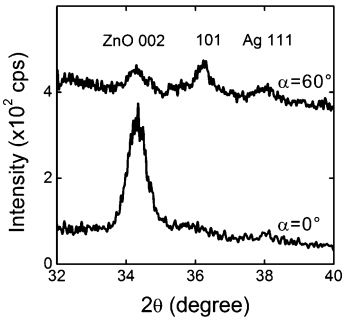

Fig. 3. XRD patterns for the annealed composites. The top and the bottom patterns correspond to the composites with $\alpha = 60$ and 0°, respectively. The data for the composite with $\alpha = 60°$ were vertically shifted by 300 cps for the sake of clarity.

ascribed to fcc Ag and wurtzite-type ZnO without any other impurity phase. The patterns indicate different ZnO orientations in the composites; when $\alpha = 0°$, only the 002 peak is seen, while both 101 and 002 peaks are observed when $\alpha = 60°$.

Figure 4 shows the cross section STEM images for the annealed composites with $\alpha = 60$ and 0°. The upper and lower images correspond to signals from bright field (BF) and HAADF detectors, respectively, taken from the same sample region. Ag and ZnO regions are clearly distinguishable in both images with inverted contrast. The HAADF image intensity approximately scales with the square of the atomic number, thus the heavy Ag particles appear brightest. Regions of strong electron scattering appear dark in the BF image, such as the Ag particles, but relatively light elements such as the SiO_2 substrate are more

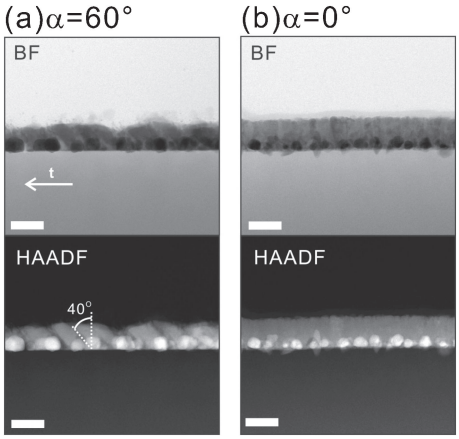

Fig. 4. STEM images for the annealed composites deposited with $\alpha = 60°$(a) and 0°(b). Upper panels correspond to the bright field (BF) images, and lower panels are the high angle angular dark field (HAADF) images. The arrow in the BF image in (a) indicates the direction of the tilt during the oblique deposition. The dotted lines in the HAADF image in (a) indicate the growth angle of the ZnO pillars from the normal to the substrate. Scale bars = 100 nm.

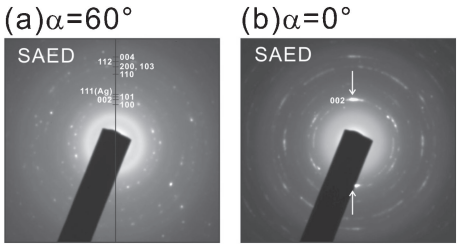

Fig. 5. The SAED patterns taken by the TEM from the comparable regions of the cross section of the annealed composites deposited with $\alpha = 60°$(a) and 0°(b). The indices of diffraction of fcc Ag and wurtzite ZnO are superimposed on the patterns. The cross section of the specimens is perpendicular to the direction of the tilt. The arrows in (b) highlight strong 002 diffraction spots from the preferred orientation of ZnO.

easily discerned. For $\alpha = 0°$, ZnO pillars grow vertically on the top of the Ag nanoparticles, while an oblique growth of ZnO pillars is clearly observed when $\alpha = 60°$. The inclined angle of the pillars with respect to the substrate is around 40° [see Fig. 4(a)], which is lower than the deposition angle of $\alpha = 60°$. For the oblique angle deposition of ZnO, the direction of growth of ZnO is often discrepant from the direction toward the source, and hence, the inclined angle is significantly less than the deposition angle,[11)–15)] because of the strong tendency of ZnO to grow with *c*-axis orientation vertically to the substrate. In the present study, we achieved well-distinct and inclined ZnO pillars thanks to the strong shadowing effect of the Ag nanoparticles dispersed on the substrate, i.e., the nanoparticles give local scaffolds for ZnO to grow obliquely.

Figure 5 shows the SAED patterns taken by the TEM from comparable regions of the cross section of the two composites. It is noted that the cross section of the TEM specimens is perpendicular to the direction of the tilt, i.e., compared to the specimens for the STEM observation, it is rotated by 90°. Diffraction patterns ascribable to ZnO are observed for both composites. The $\alpha = 60°$ composite exhibits no clear preferential orientation; the ZnO diffraction spots positioned randomly along rings corresponding to the ZnO planar spacings. In contrast, the $\alpha = 0°$ composite shows a clear preferential orientation, and two intense

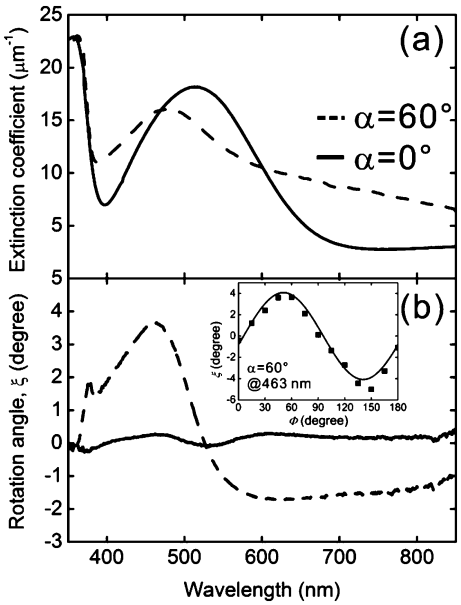

Fig. 6. (a) Optical extinction spectra for the annealed composites. Dashed and solid lines correspond to the composites deposited with $\alpha = 60$ and 0°, respectively. (b) The rotation angle of the polarization plane of transmitted light, ξ, for the annealed composites at the azimuth $\Phi = 45°$. Dashed and solid lines correspond to the composites deposited with $\alpha = 60$ and 0°, respectively. The inset shows the dependence of ξ on Φ for the composite with $\alpha = 60°$ at the wavelength of 463 nm. A solid curve is the result of fitting of Eq. (1) to the data.

spots are seen on the ring (indicated by arrows) corresponding to the 002 diffraction. A comparison with the BF TEM images taken from the same sample region (not shown here) indicates that the 002 direction corresponds to the film normal, showing that when $\alpha = 0°$, the ZnO pillars are *c*-axis oriented and grow vertically to the substrate.

Both the XRD and SAED patterns indicate that when $\alpha = 0°$, the *c*-axis of the ZnO is predominantly perpendicular to the substrate. Highly *c*-axis oriented growth of ZnO has been observed when fabricating ZnO films by PLD on not only single crystalline substrates but also glass substrates.[16)–18)] The present result indicates that this tendency holds even when the substrate is not flat but has local curvatures due to the nanoparticles. In contrast, when $\alpha = 60°$ the intensity of 002 peak in the XRD pattern is much weaker compared to the other composite. It should be noted that under the geometry adopted to measure the XRD here, only the lattice planes parallel to the substrate satisfy the diffraction condition and are detected. Thus, the absence of intense 002 peak is compatible with the morphology of inclined ZnO pillars observed in the composite with $\alpha = 60°$ [see STEM images in Fig. 4(a)].

3.2 Optical and birefringence properties of the composites

Figure 6(a) shows the optical extinction of the annealed composites. Both of the composites with $\alpha = 0°$ (represented by solid line) and 60° (dashed line) have the extinction peak around 350 nm, which is ascribed to the exciton formation in ZnO. The composites exhibit another peak at a longer wavelength, i.e., at 514 nm ($\alpha = 0°$) and 479 nm ($\alpha = 60°$), corresponding to the LSPRs of the Ag nanoparticles. The peak wavelength is shorter for the composite with $\alpha = 60°$, indicating its lower effective refractive index around the nanoparticles. The broader LSPRs of

this composite reflect a wider variation of the environment around the nanoparticles. These features in the spectra are consistent with the morphology shown in Fig. 4; the composite with $\alpha = 60°$ appears to be porous and possesses in-plane anisotropy around the Ag nanoparticles. The porous morphology reduces the effective refractive index. The in-plane anisotropy makes the optical response dependent on the polarization of incident light, which results in the broader extinction because unpolarized light was used in the experiment.

The impact of in-plane anisotropy on the macroscopic optical response is further evaluated by the rotation of the polarization plane of linearly polarized light transmitted through the composite. Figure 6(b) shows the dispersion of optical rotation ξ for the annealed composites. The sample with $\alpha = 60°$ shows a larger $|\xi|$ reflecting its anisotropic in-plane morphology. The inset in Fig. 6(b) illustrates the variation of ξ at the wavelength $\lambda = 463$ nm as a function of Φ for the composite with $\alpha = 60°$. The rotation angle oscillates with Φ and the period of oscillation is 180°, verifying that this phenomenon comes from the birefringence;[19] in other words, this composite has two orthogonal principle axes with different index of refraction. The variation of ξ with Φ can be expressed by the relation

$$\xi = A \sin[2(\Phi - B)], \quad (1)$$

where A and B are the maximum angle of rotation and the azimuth of the principle axes, respectively. The result of fitting with $A = 4.1°$ and $B = 5.8°$ is also shown as a solid curve in the inset. The value of A is related to the difference in refractive index between ordinary and extraordinary rays, Δn, by $A = \pi \Delta n d/\lambda$ (d: sample thickness). By using $A = 4.1°$, Δn is calculated to be 0.13 at $\lambda = 463$ nm. This value is much larger than the intrinsic birefringence of wurtzite ZnO ($\Delta n = 0.017$ at $\lambda = 450$ nm[20]). Equation (1) shows that no optical rotation occurs when $\Phi = B$, i.e., the polarization plane of the incident light is parallel and perpendicular to the two orthogonal principle axes. Since we define $\Phi = 0°$ when the incident electric field is parallel to $\boldsymbol{t}$, the fitting result of $B = 5.8°$ indicates that one of the principle axes is nearly along the direction of the tilt on the substrate.

A comparison of Figs. 6(a) and 6(b) indicates that the wavelength dependence of optical rotation for $\alpha = 60°$ exhibits two local maxima associated to the extinction, one at $\lambda = 377$ nm associated to the excitons of the ZnO pillars, and the other at $\lambda = 463$ nm to the LSPRs of the Ag nanoparticles. In birefringence materials where metallic nanoparticles are dispersed, the spectral position of extinction due to the LSPRs depends on the polarization direction of the incident light, which induces the optical rotation via the Kramers-Kronig relation. This mechanism of inducing birefringence was discussed in Ref. 8) for the composite of Ag nanoparticles and iron oxide. In the present system, not only the LSPRs but also the exciton induces the optical rotation. This originates from the shape of ZnO; the absorption coefficient of the rod-shaped ZnO is different between the light polarized along the short and long axes,[21] and thus the number density of the excitons created upon irradiation depends on the polarization direction relative to the orientation of the ZnO pillars.

4. Summary

We have fabricated a composite of Ag nanoparticles and ZnO pillars by using oblique angle deposition and post annealing. XRD, TEM, and STEM were used to characterize the structure and morphology of the composites; the ZnO pillars are *c*-axis oriented, and obliquely grown on the top of the Ag nanoparticles. The inclined ZnO pillar morphology of the composite is consistent with its macroscopic optical response; it brings about the polarization dependence of the optical extinction and the index of refraction. This work verifies that the present fabrication technique is simple and versatile, yet can produce a variety of composites possessing macroscopic anisotropy with relatively large dimensions.

Acknowledgments This work was supported by a Grant-in-Aid for Scientific Research (B, No. 24350104 and C, No. 24560824) and for Challenging Exploratory Research (No. 24656385) from the Ministry of Education, Culture, Sports, Science and Technology (MEXT), Japan. S. Murai and T. Matoba are also grateful for Young Researcher Overseas Visits Program for Vitalizing Brain Circulation of Japan Society for the Promotion of Science (JSPS).

References

1) S. A. Maier, "Plasmonics: Fundamentals and Applications", Springer, New York (2007).
2) T. Motohiro and Y. Taga, *Appl. Opt.*, **28**, 2466–2482 (1989).
3) N. A. Mirin and N. J. Halas, *Nano Lett.*, **9**, 1255–1259 (2009).
4) E. Plum, V. A. Fedotov, A. S. Schwanecke and N. I. Zheludev, *Appl. Phys. Lett.*, **90**, 223113 (2007).
5) J. Sung, M. Sukharev, E. M. Hicks, R. P. Van Duyne, T. Seideman and K. G. Spears, *J. Phys. Chem. C*, **112**, 3252–3260 (2008).
6) A. Dolatshahi-Pirouz, D. S. Sutherland, M. Foss and F. Besenbacher, *Appl. Surf. Sci.*, **257**, 2226–2230 (2011).
7) Y. Lei, S. Yang, M. Wu and G. Wilde, *Chem. Soc. Rev.*, **40**, 1247–1258 (2011).
8) S. Murai, T. Tsujiguchi, K. Fujita and K. Tanaka, *Opt. Express*, **19**, 23581–23589 (2011).
9) C. W. Lai, J. An and H. C. Ong, *Appl. Phys. Lett.*, **86**, 251105 (2005).
10) Z. Han, L. Ren, Z. Cui, C. Chen, H. Pan and J. Chen, *Appl. Catal., B*, **126**, 298–305 (2012).
11) I. Červeň, T. Lacko, I. Novotný, V. Tvarožek and M. Harvanka, *J. Cryst. Growth*, **131**, 546–550 (1993).
12) J. Chu, X. Peng, M. Sajjad, B. Yang and P. X. Feng, *Thin Solid Films*, **520**, 3493–3498 (2012).
13) S. Mukhtar, A. Asadov and W. Gao, *Thin Solid Films*, **520**, 3453–3457 (2012).
14) Y. W. Sun and Y. Y. Tsui, *Opt. Mater.*, **29**, 1111–1114 (2007).
15) R. Teki, T. C. Parker, H. Li, N. Koratkar, T.-M. Lu and S. Lee, *Thin Solid Films*, **516**, 4993–4996 (2008).
16) S. Hayamizu, H. Tabata, H. Tanaka and T. Kawai, *J. Appl. Phys.*, **80**, 787–791 (1996).
17) F. K. Shan, G. X. Liu, W. J. Lee, G. H. Lee, I. S. Kim, B. C. Shin and Y. C. Kim, *J. Cryst. Growth*, **277**, 284–292 (2005).
18) T. Yoshida, T. Tachibana, T. Maemoto, S. Sasa and M. Inoue, *Appl. Phys., A Mater. Sci. Process.*, **101**, 685–688 (2010).
19) K. Konishi, T. Sugimoto, B. Bai, Y. Svirko and M. Kuwata-Gonokami, *Opt. Express*, **15**, 9575–9583 (2007).
20) W. J. Tropf, M. E. Thomas and T. J. Harris, in "Handbook of Optics, 2nd edition", Vol. 2, Ed. by Michael Bass, McGraw-Hill, NewYork (1994) Chap. 33.
21) C. F. Bohren and D. L. Hoffman, "Absorption and Scattering of Light by Small Particles", Wiley, New York (1983) Chap. 8.4 p. 194.